IOP Publishing Physica Scripta
Phys. Scr. 95 (2020) 055810 (9pp) https://doi.org/10.1088/1402-4896/ab63ec

Thermopower of double-barrier magnetic tunnel junctions with a middle $La_{0.7}Sr_{0.3}MnO_3$ layer

Reza Daqiq

Department of Physics, Faculty of Science, Malayer University, Malayer, Iran

E-mail: mrdgh1@gmail.com

Received 16 July 2019, revised 17 December 2019
Accepted for publication 19 December 2019
Published 5 March 2020

Abstract

Magnetic tunnel junctions (MTJs) are promising devices for heat-assisted magnetic recording technology. Quantum transport of nanoscale double-barrier MTJs with a middle $La_{0.7}Sr_{0.3}MnO_3$ (LSMO) layer (DBMTJs-LSMO) is investigated by the non-equilibrium Green's function formalism. The thermopower is described in the linear response regime. The results of the DBMTJs-LSMO show an enhancement of the thermopower compared to DBMTJs-CoFeB and conventional single-barrier MTJs (SBMTJs) due to the LSMO physical properties and also the existence of the quantum-well (QW) states. The parallel (P) and anti-parallel (AP) thermopower of $S_P \approx -225\ \mu VK^{-1}$ and $S_{AP} \approx -320\ \mu VK^{-1}$ are achieved at room temperature for DBMTJs-LSMO. The tunnel magneto-thermopower ratio is found to be 42% at room temperature along with its maximum value of 138% at $T = 163$ K for DBMTJs-LSMO.

Keywords: thermopower, double-barrier MTJs, LSMO, quantum-well states

(Some figures may appear in colour only in the online journal)

1. Introduction

Thermoelectricity of nanoscale systems has been investigated by theoretical and experimental research [1, 2]. Seebeck showed that waste heat can be converted into electricity in thermoelectric (TE) materials.

In order to investigate efficiency of a TE material, a dimensionless figure of merit $ZT = S^2GT/(\lambda_{el} + \lambda_{ph})$ is used in which S denotes the thermopower, G the electrical conductance, T the average temperature and $\lambda_{el}(\lambda_{ph})$ the electronic (phononic) contribution to the thermal conductance [3]. The potential of a TE material with high figure of merit is a dare for theoretical and experimental research [4].

Magnetic tunnel junctions (MTJs) can be used as the basic unit for heat-assisted magnetic recording (HAMR) media [5, 6]. MgO-based MTJs are more appealing due to high tunnel magneto-Seebeck (TMS) ratio [7–10] and tunnel magneto-resistance (TMR) [11]. The TMS in the MTJs is a spin caloritronics effect that provides the feasibility to acquire thermovoltages depending on the magnetic configuration of the MTJs. The different values of the thermopower have been observed in the MgO-based MTJs [12, 13].

Double-barrier MTJs (DBMTJs) are significant in spintronic devices due to the existence of the quantum-well (QW) states inside the middle layer. The large TE effects can be achieved by resonant tunneling from the QW states [14, 15]. Once the resonant states shift to the Fermi energy, the energy dependence of the transmission shows asymmetric behavior and as a result, the thermopower increases.

It is possible to control the position of the resonant states by an external magnetic field in the DBMTJs including a middle ferromagnetic (FM) material. Therefore, the TE effects can be changed using an external magnetic field.

Perovskite manganites $La_{1-x}A_xMnO_3$ (where A = Sr, Ba, Ca) with huge magnetoresistance have shown diverse physical circumstances due to multiple couplings among charge, spin and degrees of freedom [16]. To explain the transport mechanism through the $La_{1-x}A_xMnO_3$, different models [17–19] have been formed. Interfacial effects on the TMR are investigated in a combination of $La_{0.7}Sr_{0.3}MnO_3$

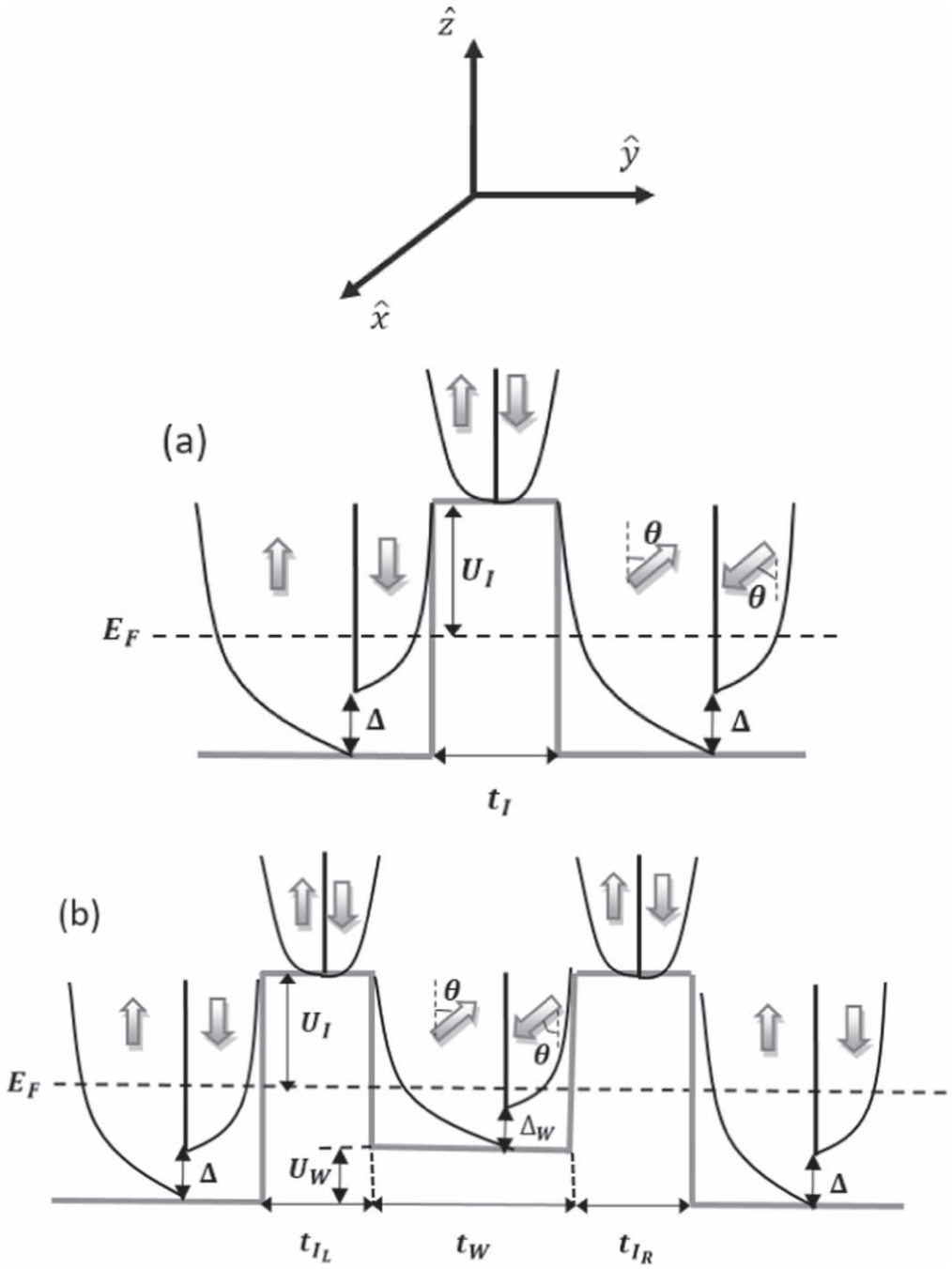

Figure 1. Conduction-band profile of (a) single-barrier magnetic tunnel junctions (SBMTJs) CoFeB/MgO/CoFeB and (b) double-barrier magnetic tunnel junctions with a middle LSMO layer (DBMTJs-LSMO) CoFeB/MgO/LSMO/MgO/CoFeB. The magnetizations of the left and right CoFeB contacts are fixed at parallel configuration while that of the LSMO layer makes an angle θ with the z-axis. The spin-splitting of the CoFeB contacts is Δ and that of the LSMO layer is Δ_W. The barrier height of the MgO insulators above the Fermi energy E_F is U_I and the conduction-band offset of the LSMO layer is U_W. The thickness of the MgO insulator is t_I for the SBMTJs and those of the left (right) MgO insulator, middle LSMO layer are$t_{I_{L(R)}}$, t_W respectively.

(LSMO) with the MgO insulator as LSMO/MgO/Fe tunneling junction, experimentally [20]. The combination of the perovskite manganites for example LSMO with MgO barriers may lead to stimulating effects because of the different lattice structures as well as the high degree of epitaxial strain in such interface. Effects of nanostructure on TE properties of synthesized LSMO compound are also studied recently in a definite range of temperatures [21].

The purpose of present work is to investigate the thermopower of the DBMTJs with structures as CoFeB/MgO/CoFeB/MgO/CoFeB (DBMTJs-CoFeB). The junctions are based on an FM material (e.g. CoFeB) as a quantum well between two MgO insulators as barriers and surrounded by two CoFeB contacts (figure 1). To improve the thermopower of the DBMTJs-CoFeB, the middle CoFeB layer is replaced by an LSMO layer (DBMTJs-LSMO). The thermopower of

the DBMTJs-LSMO is also compared to that of single-barrier MTJs (SBMTJs).

Some DBMTJs such as Fe/MgO/Fe/MgO/Fe [22], CoFeB/MgO/CoFe/MgO/CoFeB [23] are investigated experimentally. However, experimental investigations in the DBMTJs-LSMO have not yet been reported. It is to be noted that LSMO/MgO/Fe tunneling junctions are grown by magnetron sputtering recently [20].

This paper is organized as follows. Section 2 describes the details of the model and formalism. In section 3 the method is used to investigate the structures. The conclusions are presented in section 4.

2. Model and formalism

A two terminal nanoscale device is considered in the linear response regime as the temperature difference between the left (L) and right (R) contacts of $\Delta T (=T_L - T_R)$ is assumed to be very small. The electric current (I_e) is given by [3, 24]:

$$I_e = \frac{e^2}{h}\left(L_0 \Delta V - \frac{k_B T}{e} L_1 \frac{\Delta T}{T}\right), \tag{1}$$

where h represents the Planck's constant, ΔV the applied voltage (induced byΔT), k_B the Boltzmann's constant, and $T = (T_L + T_R)/2$ average temperature.

The thermopower (S) for zero electric current ($I_e = 0$) is calculated by:

$$S = \lim_{\Delta T \to 0}\left(\frac{\Delta V}{\Delta T}\right) = \left(-\frac{k_B}{e}\right)\frac{L_1}{L_0}, \tag{2}$$

where dimensionless coefficients $L_n (n = 0, 1)$ are defined as:

$$L_n = \int_{-\infty}^{+\infty}\left(\frac{E - E_F}{k_B T}\right)^n \mathcal{T}(E)\left(-\frac{\partial f}{\partial E}\right) \mathrm{d}E. \tag{3}$$

The symbol $\mathcal{T}(E)$ denotes electronic transmission and $f(E, T) = [\exp((E - E_F)/k_B T) + 1]^{-1}$ the Fermi-Dirac distribution function.

The tunnel-magneto thermopower (TMT) ratio through the MTJs is given by [25]:

$$\mathrm{TMT} = \frac{S_\mathrm{P} - S_\mathrm{AP}}{\min(|S_\mathrm{P}|, |S_\mathrm{AP}|)} \times 100. \tag{4}$$

In the present work, a quantum mechanical model describes the flow of electrons coherently through the junctions. It is assumed that all dissipative and phase-breaking processes to be limited to the contacts.

To calculate the electronic transmission, a single-band effective mass Hamiltonian is used in the non-equilibrium Green's function (NEGF) formalism [26–28]. The Hamiltonian is written as:

$$H = H_0 \hat{I} - (\boldsymbol{\sigma}.\boldsymbol{m})\frac{\Delta_i}{2}, \tag{5}$$

where H_0 is spin-independent part and $\hat{I}$ the 2×2 identity matrix. The diagonal and off-diagonal elements of the H_0 matrix are corresponding to the on-site potentials and coupling energies (between nearest-neighbor sites), respectively:

$$\varepsilon_i = 2\tau_i + E_{C_i} \tag{6}$$

$$\tau_i = \frac{-\hbar^2}{2m_i^* a^2}, \tag{7}$$

where $i \in$ CoFeB, MgO, LSMO regions and E_C denotes the conduction band edge (with respect to the bottom of the conduction band of the CoFeB contacts), $\hbar$ the reduced Planck's constant, a lattice spacing and m^* effective mass. The interface energies can be written as$(\tau_i + \tau_j) + (E_{C_i} + E_{C_j})/2$, where $i, j \in$ CoFeB, MgO, LSMO regions.

The second term of the Hamiltonian is spin-dependent part in which $\boldsymbol{\sigma} = (\sigma_x, \sigma_y, \sigma_z)$ the Pauli's spin vector, $\boldsymbol{m}$ the free magnet direction and Δ_i the spin-splitting of the ferromagnetic materials where$i \in$ CoFeB, LSMO regions.

In the NEGF formalism, the Green's function ($\mathcal{G}$) is defined as:

$$\mathcal{G}(E) = [E\hat{I} - H - \Sigma_L - \Sigma_R]^{-1}. \tag{8}$$

In equation (8), E denotes the electron energy and $\Sigma_{L(R)}$ the 2×2 left (right) self-energy matrix of the CoFeB contacts:

$$\Sigma_{L,R}(i, i, k_\parallel) = \begin{bmatrix} -t_{\mathrm{CoFeB}}\exp(\mathrm{i}k_j^{\uparrow} a) & 0 \\ 0 & -t_{\mathrm{CoFeB}}\exp(\mathrm{i}k_j^{\downarrow} a) \end{bmatrix}, \tag{9}$$

where $\boldsymbol{k}_\parallel = (k_x, k_z)$ denotes the transverse wave vector and $k_j^{\uparrow(\downarrow)}$ are the wave vectors of the spin up (down) electrons [26, 27].

The electronic transmission is given by the Landauer–Büttiker formula:

$$\mathcal{T}(E) = Tr[\Gamma_L(E)\mathcal{G}(E)\Gamma_R(E)\mathcal{G}^\dagger(E)], \tag{10}$$

where the broadening matrix of the left (right) contacts $\Gamma_{L(R)}$ is defined as:

$$\Gamma_{L(R)}(E) = \Delta(\Sigma_{L(R)} - \Sigma_{L(R)}^\dagger). \tag{11}$$

To calculate 3D transmission, it has summed over the first 50 transverse energies (modes) of $E_\parallel = \hbar^2 k_\parallel^2/2m^*$ in the xz plane.

The periodic boundary conditions are assumed in the transverse direction as the transverse modes are decoupled like individual 1D wires. It is also assumed that the transverse wave vector $k_\parallel$ for each transverse mode conserves throughout the structure. The transverse energies in the CoFeB contacts, MgO barriers and LSMO layer are different because of dissimilarity in the effective masses.

The barriers are improbable to be defect free over the junction area of the real MTJs due to surface imperfections and lattice mismatch between Fe and MgO [11] and these factors lead to non-conservation of $k_\parallel$, however are outside of this work.

3. Results and discussions

The material parameters for the CoFeB contacts, MgO insulators and LSMO layer are: the Fermi energy of the CoFeB contacts $E_F = 2.25$ eV [27], the effective mass for electrons

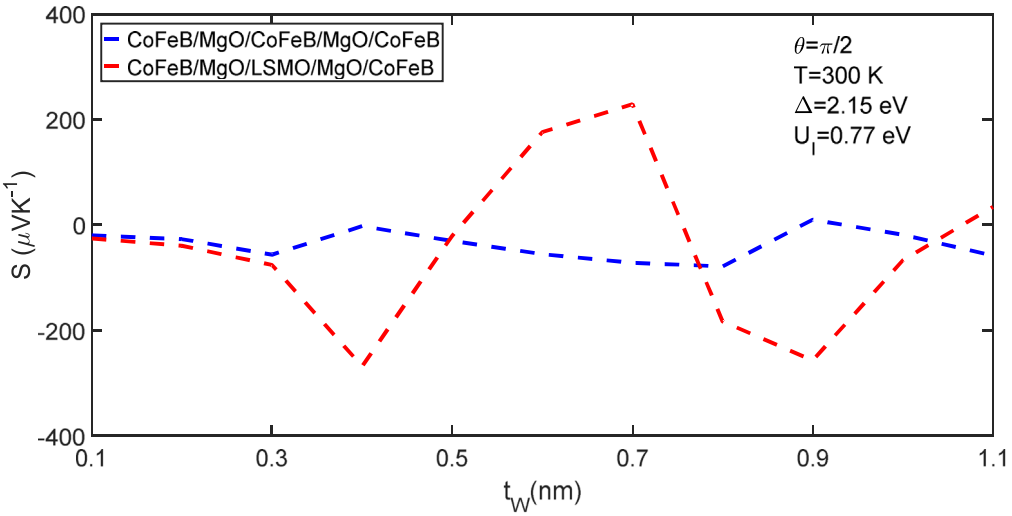

Figure 2. The thermopower as a function of the middle layer thickness (t_W) for DBMTJs-LSMO and DBMTJs-CoFeB with $t_{I_L} = t_{I_R} = 0.5$ nm at$\theta = \pi/2$, $\Delta = 2.15$ eV, $U_I = 0.77$ eV, $T = 300$ K.

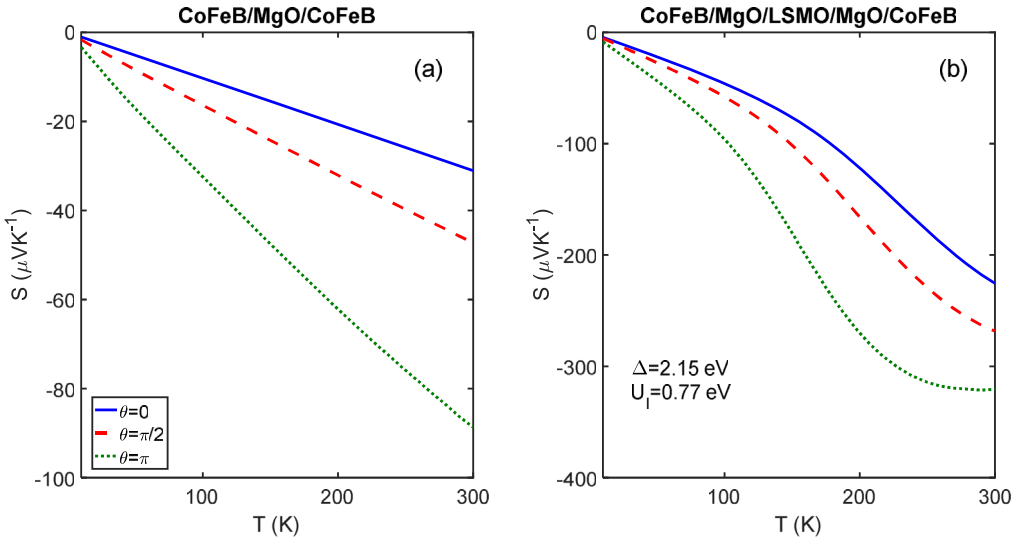

Figure 3. The thermopower as a function of the average temperature (T) for SBMTJs (a) with $t_I = 1.4$ nm and DBMTJs-LSMO (b) with $t_W = 0.4$ nm, $t_{I_L} = t_{I_R} = 0.5$ nm at $\theta = 0, \pi/2, \pi$, $\Delta = 2.15$ eV, $U_I = 0.77$ eV.

inside the CoFeB contacts $m^*_{\mathrm{CoFeB}} = 0.8\, m_{\mathrm{e}}$ (m_e is mass of free electron) [27], the spin-splitting of the CoFeB contacts $\Delta = 2.15$ eV [27], the barrier height of the MgO insulators above the Fermi energy $U_I = 0.77$ eV [27], the effective mass for electrons inside the MgO insulators $m^*_{\mathrm{MgO}} = 0.18\ m_e$ [27], the conduction-band offset of the LSMO layer $U_W = 1.90$ eV [26], the LSMO spin-splitting $\Delta_W = 0.7$ eV [26] and the effective mass for electrons inside the LSMO layer $m^*_{\mathrm{LSMO}} = 4\, m_e$ [29]. The spin-splitting of the MgO barriers is zero in the present calculation.

Figure 2 shows the thermopower as a function of the middle layer thickness (t_W) for the DBMTJs-LSMO (CoFeB) structure. With increase of t_W, the resonant peaks appear for the thermopower at the specific thicknesses of the LSMO layer (correspond to the resonant positions of the quantum well) because the thermal current (current made by thermal gradient) from the warmer to the colder contact can be balanced by the bias current (current made by bias voltage) in the opposite direction between the contacts. Therefore, the annulment of the thermal current at a resonant position requires a large bias voltage as it leads to a significant increase of the thermopower.

The results show that the thermopower is larger for the DBMTJs-LSMO than that of the DBMTJs-CoFeB because the transmission in the former is larger than that in the latter due to the non-zero conduction-band offset (U_W).

Once the thickness of the inserted CoFeB (LSMO) changes, the position of the resonant peaks (related to the QW states) in the transmission can be shifted to the Fermi level and it leads to the large thermopower.

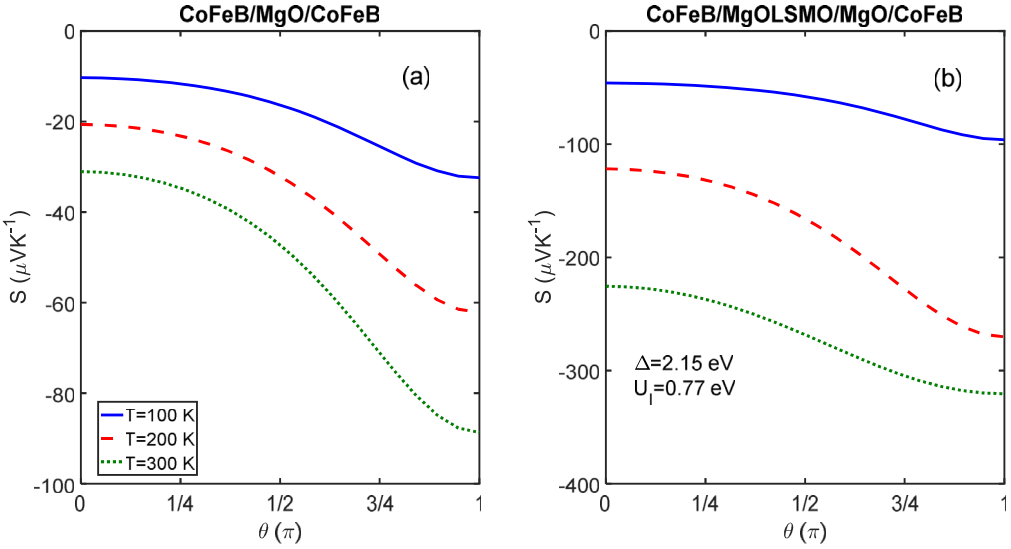

Figure 4. Angular dependence of the thermopower for SBMTJs (a) with $t_I = 1.4$ nm and DBMTJs-LSMO (b) with $t_W = 0.4$ nm, $t_{I_L} = t_{I_R} = 0.5$ nm at $T = 100$ K, 200 K, 300 K, $\Delta = 2.15$ eV, $U_I = 0.77$ eV.

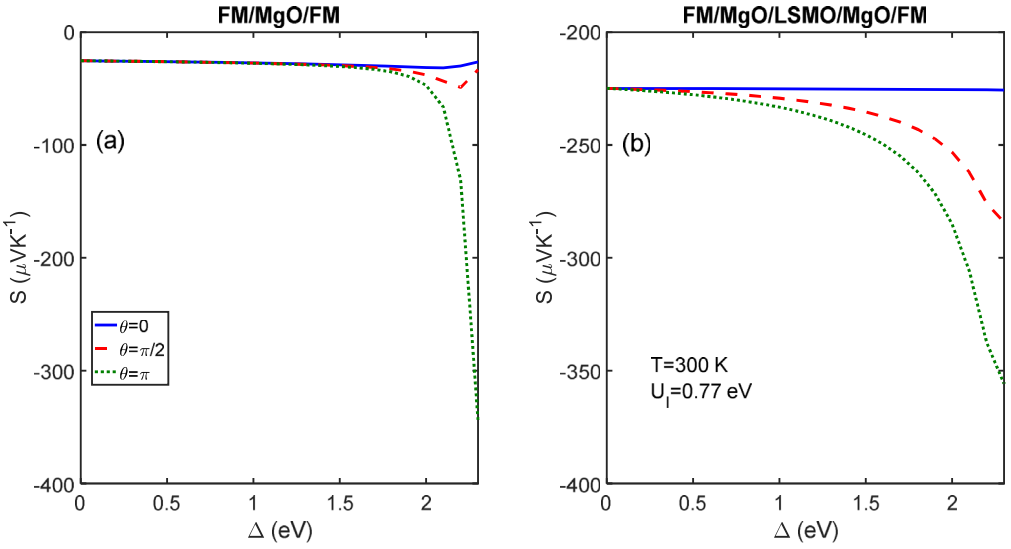

Figure 5. The thermopower as a function of the spin-splitting (Δ) for FM/MgO/FM (a) with $t_I = 1.4$ nm and FM/MgO/LSMO/MgO/FM (b) with $t_W = 0.4$ nm, $t_{I_L} = t_{I_R} = 0.5$ nm at $\theta = 0, \pi/2, \pi$, $T = 300$ K, $U_I = 0.77$ eV.

The thermopower shows positive and negative values which are related to the transmission ($\mathscr{T}(E)$) with energies lower and higher than the Fermi energy ($E < E_F$ and $E > E_F$), respectively.

The same thickness of the middle region ($t_{I_L} + t_W + t_{I_R} = 1.4$ nm) for the DBMTJs-LSMO and ($t_I = 1.4$ nm) for the SBMTJs are considered in figures 3–7.

The temperature and angular dependence of the thermopower for DBMTJs-LSMO and SBMTJs are plotted in figures 3 and 4, respectively. The thermopower increases for elevated temperatures and its magnitude at the anti-parallel (AP) configuration is greater than that of parallel (P) configuration which is shown in the MTJs from first-principle calculations [25]. The thermal current increases more significantly with temperature than the bias current and as a result larger bias between the contacts is necessary at higher temperatures for zero electric current in the MTJs.

A deviation from linear form with increase of temperature is found for the DBMTJs-LSMO. The P and AP thermopower of $S_{\rm P} \approx -225\ \mu{\rm VK}^{-1}$and $S_{\rm AP} \approx -320\ \mu{\rm VK}^{-1}$ are achieved at room temperature for double-barrier structure.

For the MgO-based SBMTJs, the thermopower is also calculated of $S_{\rm P} = -12\ \mu{\rm VK}^{-1}$, $S_{\rm AP} = -15\ \mu{\rm VK}^{-1}$ in the MgO-based SBMTJs for $t_I = 2.6$ nm [13] while the present result is $S_{\rm P} \approx -32\ \mu{\rm VK}^{-1}$, $S_{\rm AP} \approx -89\ \mu{\rm VK}^{-1}$ at room temperature for $t_I = 1.4$ nm.

The angular dependence shows that the thermopower in the AP configuration is larger than that in the others. Both the thermal current and bias current are maximum in the P configuration. On the other hand, the bias current decreases

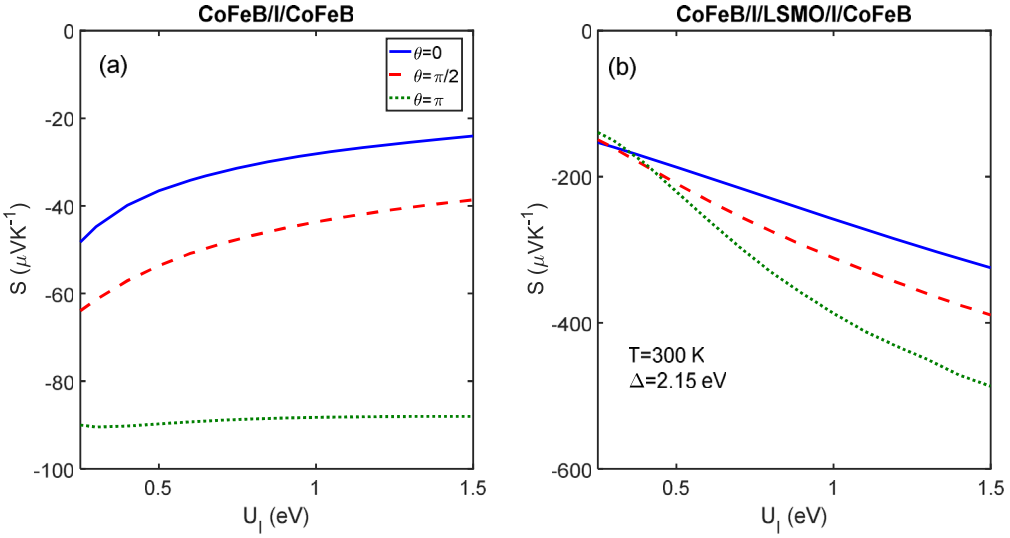

Figure 6. The thermopower as a function of the barrier height (U_I) for CoFeB/I/CoFeB (a) with $t_I = 1.4$ nm and CoFeB/I/LSMO/I/CoFeB (b) with $t_W = 0.4$ nm, $t_{I_L} = t_{I_R} = 0.5$ nm at $\theta = 0$, $\pi/2$, π, $T = 300$ K, $\Delta = 2.15$ eV.

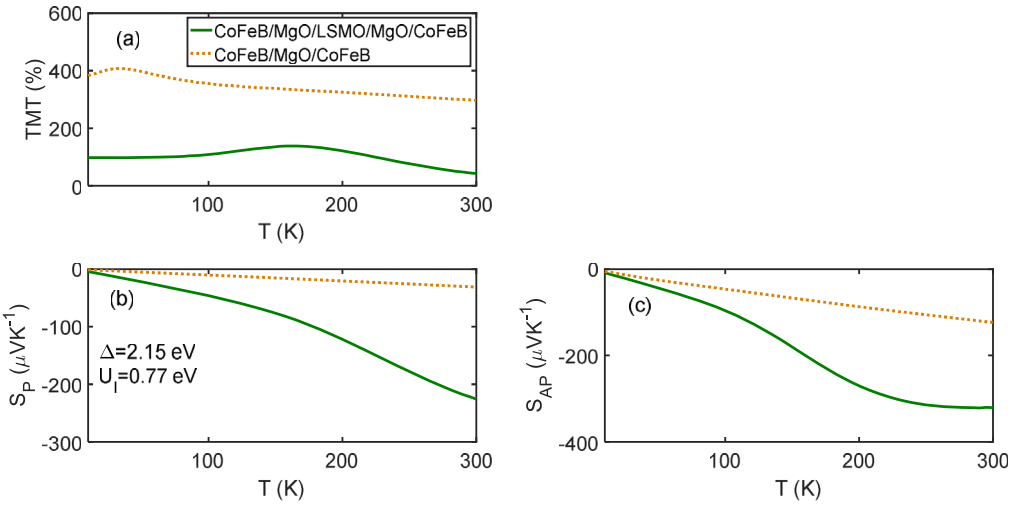

Figure 7. The TMT ratio (a), thermopower at parallel configuration (S_P) (b) and thermopower at anti-parallel configuration (S_{AP}) (c) as a function of average temperature (T) for DBMTJs-LSMO with $t_W = 0.4$ nm, $t_{I_L} = t_{I_R} = 0.5$ nm and SBMTJs with $t_I = 1.4$ nm at $\Delta = 2.15$ eV, $U_I = 0.77$ eV.

significantly with alteration of magnetic configuration from the P to AP of that. As a result, a higher bias is necessary to decrease the electric current to zero in the AP configuration than that of the P configuration and the thermopower is maximum in the AP configuration. The different effects of the magnetic configurations on the currents are explained by the point that the tunneling electrons of the thermal current from the warmer to colder contact have higher energies than those of the bias current in the direction perpendicular to the barrier.

The thermopower changes gradually from the P configuration to the perpendicular configuration and rapidly from the perpendicular configuration to the AP configuration in agreement with a previous work [30]. There are also deviations from cos θ dependence [31].

It is also observed that the presence of the QW states and the resonant tunneling cause to an increase of the thermopower for the DBMTJs-LSMO compared to that of the SBMTJs at the same structural characteristics.

The junctions including unknown materials for the FM contacts and insulators (I) (except for the CoFeB contacts and MgO insulators) are also investigated.

Influence of an increase in the spin-splitting contacts on the thermopower is shown in figure 5. The spin polarization of the tunneling electrons increases with increase of the spin-splitting. The thermopower usually increases as the spin-splitting increases. For the FM contacts with large spin-splitting, the bias current can be strongly decreased because of a strong reduction in the density of states for minority electrons near to the Fermi energy. Such reduction has less impact

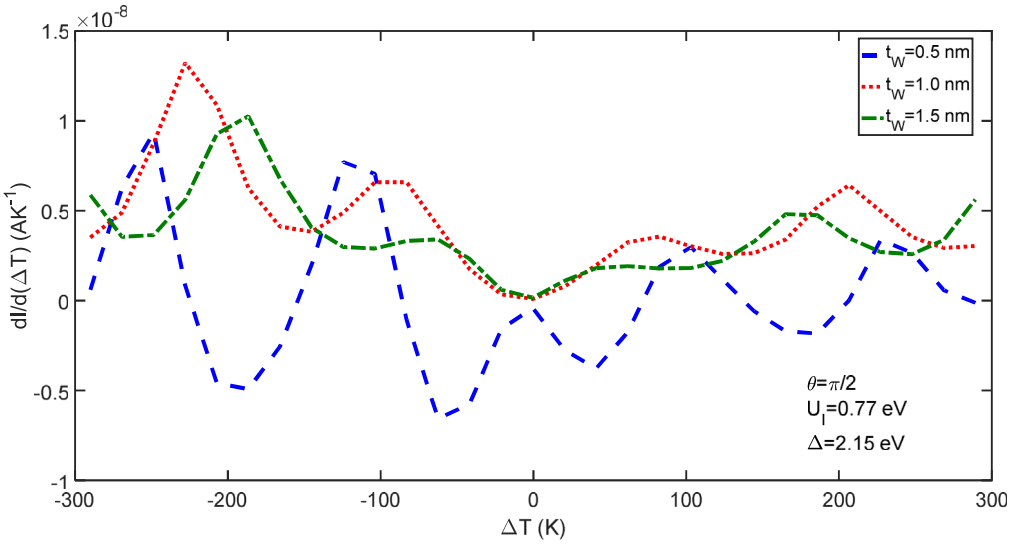

Figure 8. Differential conductance as a function of the temperature difference of the left and right contacts for the DBMTJs-LSMO with $t_W = 0.5$ nm, 1.0 nm, 1.5 nm, $t_{I_L} = t_{I_R} = 0.5$ nm at $\Delta = 2.15$ eV, $U_I = 0.77$ eV, $\theta = \pi/2$. Other parameters are considered from [36].

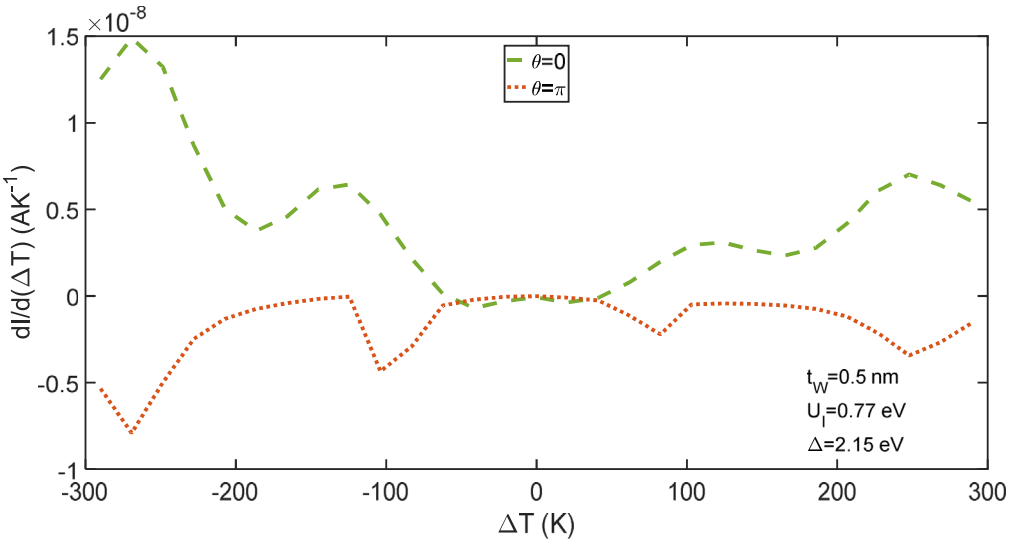

Figure 9. Differential conductance as a function of the temperature difference of the left and right contacts ΔT for the DBMTJs-LSMO with $t_W = t_{I_L} = t_{I_R} = 0.5$ nm at $\Delta = 2.15$ eV, $U_I = 0.77$ eV, $\theta = 0,\ \pi$. Other parameters are considered from [36].

on the tunneling electrons from the contact with higher temperature to the other for energies higher than the Fermi energy ($E > E_F$) and these electrons have significant contributions in the thermal current.

Figure 6 shows the thermopower as a function of the barrier height for the DBMTJs-LSMO and SBMTJs. With a reduction in the barrier height, an increase of the transmission is found for electrons with higher energy than the others which leads to an increase of the thermopower for the SBMTJs.

With increase of the barrier height, the resonance energies also increase for the DBMTJs-LSMO because of the confinement effects through the DBMTJs and as a result, the transmission increases for electrons with higher energy.

The changing of the thermopower through the magnetization switching from the P configuration to the AP configuration is described by the TMT ratio which is plotted in figure 7. The TMT ratio is positive and large because of $|S_{AP}| > |S_P|$ for both junctions, however, it is larger in the SBMTJs than that in the DBMTJs-LSMO. The TMT ratio is found to be 42% at room temperature along with its maximum value of 138% at $T = 163$ K for the DBMTJs-LSMO.

For the initial observation, the TMT ratios are found to be 90% [7] and −8.8% [8] in the MgO-based MTJs. The TMT ratio of several 1000% (with temperature dependence) is predicted theoretically [9] and a full review of the TMS magnitudes for devices and future applications is presented recently [10]. The dependence of the laser-induced TMT on the MgO barrier thickness is investigated with TMT ratio from around 15% to 28% [13]. The TMS ratio of −95% is reported experimentally in the MTJs with half-metallic

Heusler contacts [32]. In the present work, the maximum TMT ratio is found to be 408% at $T = 31$ K for the SBMTJs.

In addition the parameters discussed in the present work, other parameters can also be affected the TE effects such as strain and stress [33, 34], electric bias [35], and so on.

Figure 8 shows the differential conductance $\mathrm{d}I/\mathrm{d}(\Delta T)$ in the nonlinear response regime [36] for the DBMTJs-LSMO. Some strong oscillations of conductance (quantum effects) are found in the negative region while the oscillation amplitude slightly attenuates with the sign change of ΔT for a certain thickness of the QW. Such oscillations have different periodicity for different thicknesses of t_W. With increase of t_W, the oscillatory feature decreases which is expected in the double-barrier structures.

To complete the present discussion, the differential conductance $\mathrm{d}I/\mathrm{d}(\Delta T)$ as a function of ΔT is plotted in figure 9 for the DBMTJs-LSMO at the P ($\theta = 0$) and AP ($\theta = \pi$) configurations. It is observed that there is almost no oscillatory feature for the small values of ΔT as the application of a higher thermal gradient to the DBMTJs [37] results in an increase of the oscillatory feature for the P and AP configurations. An attenuation of the oscillation amplitude is observed with increase of temperature in a recent work [37] like to that in the present work for the sign change of ΔT, however, the periodicity is nearly unchanged in the former unlike to that of the latter.

4. Conclusion

Quantum transport through the nanoscale DBMTJs-LSMO are investigated using the NEGF formalism. The thermopower is described in the linear response regime. Effects of different parameters such as inserted LSMO (CoFeB) thickness, average temperature, magnetization alignment and so on are also studied in the DBMTJs and SBMTJs. The P and AP thermopower of $S_{\mathrm{P}} \approx -225\ \mu\mathrm{VK}^{-1}$and $S_{\mathrm{AP}} \approx -320\ \mu\mathrm{VK}^{-1}$ are achieved at room temperature for DBMTJs-LSMO. The TMT ratio is found to be 42% at room temperature along with its maximum value of 138% at $T = 163$ K for the DBMTJs-LSMO. It is also found that the TMT ratio is larger in the SBMTJs than that in the DBMTJs-LSMO. The resonant QW states in the MgO-based DBMTJs lead to an increase of the thermopower compared to that of the SBMTJs.

We learn from the obtained results that the DBMTJs-LSMO can be improved the TE parameters compared to those of the conventional SBMTJs in the nanoscale devices as an MgO single-barrier can be substituted by an MgO/LSMO/MgO double-barrier at the same thicknesses. It is possible to use the resonant tunneling effect under an external magnetic field.

The present work will open up further theoretical and experimental efforts in the spin caloritronics field to design the next generations of the nano-electronic devices e.g. HAMR technology. It can be investigated next the asymmetric DBMTJs-LSMO with different barriers and FM contacts to find the improved results in future works. The idea of TE quantum transport can also be extended to the nanoscale superlattice MTJs [38].

The TMS in the DBMTJs [39] is investigated recently from theoretical point of view. However, experiments subsequent these ideas have not yet been established.

Acknowledgments

This work has not received any funding support from organizations.

ORCID iDs

Reza Daqiq https://orcid.org/0000-0001-6558-173X

References

[1] Sanchez D and Linke H 2014 Focus on thermoelectric effects in nanostructures *New J. Phys.* **16** 110201
[2] Pichard J-L and Whitney R 2016 Foreword *C. R. Phys.* **17** 1039
[3] Bevilacqua G, Grosso G, Menichetti G and Pastori Parravicini G 2016 Thermoelectric efficiency of nanoscale devices in the linear regime *Phys. Rev.* B **94** 245419
[4] Beneti J, Casati G, Saito K and Whitney R S 2017 Fundamental aspects of steady-state conversion of heat to work at the nanoscale *Phys. Rep.* **694** 1
[5] Dieny B *et al* 2018 Impact of integration spin-transfer torque due to huge thermal gradients in heat-assisted magnetic recording *IEEE Trans. Magn.* **54** 0800111
[6] Weller D, Parker G, Mosendz O, Lybratos A, Mitin D, Safonova N Y and Albrecht M 2016 Review article: FePt heat assisted magnetic recording media *J. Vac. Sci. Technol.* B **34** 060801
[7] Liebing N, Serrano-Guisan S, Rott K, Reiss G, Langer J, Ocker B and Schumacher H W 2011 Tunneling magnetothermopower in magnetic tunnel junction nanopillars *Phys. Rev. Lett.* **107** 177201
[8] Walter M *et al* 2011 Seebeck effect in magnetic tunnel junctions *Nat. Mater.* **10** 742
[9] Czerner M, Bachmann M and Heiliger C 2011 Spin caloritronics in magnetic tunnel junctions: *ab initio* studies *Phys. Rev.* B **83** 132405
[10] Kuschel T, Czerner M, Walowski J, Thomas A, Schumacher H W, Reiss G, Heiliger C and Münzenberg M 2019 Tunnel magneto-Seebeck effect *J. Phys. D: Appl. Phys.* **52** 133001
[11] Butler W H, Zhang X-G, Schultess T C and MacLaren J M 2001 Spin-dependent tunneling conductance of Fe/MgO/Fe sandwiches *Phys. Rev.* B **63** 054416
[12] Huebner T, Boehnke A, Martens U, Thomas A, Schmalhorst J, Reiss G, Münzenberg M and Kuschel T 2016 Comparison of laser-induced and intrinsic tunnel magneto-Seebeck effect in CoFeB/$MgAl_2O_4$ and CoFeB/MgO magnetic tunnel junctions *Phys. Rev.* B **93** 224433
[13] Huebner T, Martens U, Walowski J, Boehnke A, Krieft J, Heiliger C, Thomas A, Reiss G, Kuschel T and Münzenberg M 2017 Enhancement of thermovoltage and tunnel magneto-Seebeck effect in CoFeB-based magnetic tunnel junctions by variation of the $MgAl_2O_4$ and MgO barrier thickness *Phys. Rev.* B **96** 214435
[14] Teixeira J M, Costa J D, Ventura J M, Sousa J B, Wisniowski P and Freitas P P 2014 Observation of spin-dependent quantum well resonant tunneling in textured CoFeB layers *Appl. Phys. Lett.* **104** 112414

[15] Jia X, Wang S and Qin M 2016 Enhanced thermal spin transfer in MgO-based double-barrier tunnel junctions *New J. Phys.* **18** 63012
[16] Jin S, Tiefel T J, McCormack M, Fastancht R A, Ramesh R and Chen L H 1994 Thousandfold change in resistivity in magnetoresistive La–Ca–Mn–O films *Science* **264** 413
[17] Millis A J 1998 Lattice effects in mangnetoresistive manganese perovskites *Nature* **392** 147
[18] Fath M, Freiesm S, Menovsky A A, Tomioka Y, Aarts J and Mydosh J A 1999 Spatially inhomogeneous metal-insulator transition in doped manganites *Science* **285** 1540
[19] Millis A J 1996 Cooperative John–Teller effect and electron-phonon coupling in $La_{1-x}A_xMnO_3$ *Phys. Rev.* B **53** 8434
[20] Galceran R *et al* 2015 Interfacial effects on the tunneling magnetoresistance in $La_{0.7}Sr_{0.3}MnO_3$/MgO/Fe tunneling junctions *Phys. Rev.* B **92** 094428
[21] Singh S, Srivastav S K, Patel A, Chatterjee R and Pandey S K 2018 Effect of nanostructure on thermoelectric properties of $La_{0.7}Sr_{0.3}MnO_3$ in 300–600 K temperature range *Mater. Res. Express* **5** 055026
[22] Nozaki T, Tezuka N and Inomata K 2006 Quantum oscillation of the tunneling conductance in fully epitaxial double barrier magnetic tunnel junctions *Phys. Rev. Lett.* **96** 027208
[23] Liu R S *et al* 2013 CoFe alloy as middle layer for strong spin dependent quantum well resonant tunneling in MgO double barrier magnetic tunnel junctions *Phys. Rev.* B **87** 024411
[24] Butcher P N 1990 Thermal and electrical transport formalism for electronic microstructures with many terminals *J. Phys. Condens. Matter* **2** 4869
[25] Wang S-Z, Xia K and Bauer G E W 2014 Thermoelectricity and disorder of FeCo/MgO/FeCo magnetic tunnel junctions *Phys. Rev.* B **90** 224406
[26] Datta D, Behin-Aein B, Salahuddin S and Datta S 2010 Quantitative model for TMR and spin-transfer torque in MTJ devices *Int. Electron Device Meeting (IEDM)* 22.8.1
[27] Datta D, Behin-Aein B, Salahuddin S and Datta S 2012 Voltage asymmetry of spin transfer torques *IEEE Trans. Nano* **11** 261
[28] Datta S 2005 *Quantum Transport: Atom to Transistor* 1st edn (New York, USA: Cambridge University Press)
[29] Wang L M, Liu C-C, Yang H C and Horng H E 2004 Room temperature tunneling magnetoresistance in $La_{0.7}Sr_{0.3}MnO_3$ step-edge junctions *J. Appl. Phys.* **95** 4928
[30] Heiliger C, Czerner M, Liebing N, Serrano-Guisan S, Rott K, Reiss G and Schumacher H W 2018 Unusual angular dependence of tunneling magneto-Seebeck effects *AIP Adv.* **8** 115114
[31] Slonczewski J C 1989 Conductance and exchange coupling of two ferromagnets separated by a tunneling barrier *Phys. Rev.* B **39** 6995
[32] Boehnke A *et al* 2017 Large magneto-Seebeck effect in magnetic tunnel junctions with half-metallic Heusler electrodes *Nat. Commun.* **8** 1626
[33] Xu Y and Li G 2012 Strain effect analysis on the thermoelectric figure of merit in n-type Si/Ge nanocomposites *J. Appl. Phys.* **111** 054318
[34] Thonhauser T, Scheidemantel T J, Sofo J O, Badding J V and Mahan G D 2003 Thermoelectric properties of Sb_2Te_3 under pressure and uniaxial stress *Phys. Rev.* B **68** 085201
[35] Tiusan C, Faure-Vincent J, Bellouard C, Hehn M, Jouguelet E and Schuhl A 2004 Interfacial resonance state probed by spin-polarized tunneling in epitaxial Fe/MgO/Fe tunnel junctions *Phys. Rev. Lett.* **93** 106602
[36] Daqiq R 2017 Temperature gradient effects on spin torque in double barrier magnetic tunnel junctions with a non-magnetic metal spacer *J. Supercond. Nov. Magn.* **30** 1593
[37] Tao B S *et al* Long-range phase coherence in double-barrier magnetic tunnel junctions with a large thick metallic quantum well *Phys. Rev. Lett.* **115** 1572042015
[38] Sharma A, Tulapurkar A A and Muralidharan B 2018 Band-pass Fabry–Pèrot magnetic tunnel junctions *Appl. Phys. Lett.* **112** 192404
[39] Daqiq R 2018 Enhancement of thermopower by structural asymmetry in double-barrier tunnel junctions *J. Supercond. Nov. Magn.* **31** 313